Chinese Chemical Letters 36 (2025) 109857

Contents lists available at ScienceDirect

Chinese Chemical Letters

journal homepage: www.elsevier.com/locate/cclet

PD-L1 targeted iron oxide SERS bioprobe for accurately detecting circulating tumor cells and delineating tumor boundary

Ting Pan[a,1], Dinghu Zhang[a,1], Guomei You[a], Xiaoxia Wu[a,*], Chenguang Zhang[b], Xinyu Miao[a], Wenzhi Ren[b,c], Yiwei He[a], Lulu He[b], Yuanchuan Gong[a], Jie Lin[b,c,*], Aiguo Wu[b,c,*], Guoliang Shao[a,*]

[a] *Department of Interventional Radiology, Zhejiang Cancer Hospital, Institute of Basic Medicine and Cancer (IBMC), Chinese Academy of Sciences, Hangzhou 310022, China*

[b] *Ningbo Key Laboratory of Biomedical Imaging Probe Materials and Technology, Cixi Institute of Biomedical Engineering, International Cooperation Base of Biomedical Materials Technology and Application, Chinese Academy of Science (CAS) Key Laboratory of Magnetic Materials and Devices and Zhejiang Engineering Research Center for Biomedical Materials, Ningbo Institute of Materials Technology and Engineering, CAS, Ningbo 315201, China*

[c] *Advanced Energy Science and Technology Guangdong Laboratory, Huizhou 516000, China*

ARTICLE INFO

Article history:
Received 16 October 2023
Revised 28 March 2024
Accepted 2 April 2024
Available online 3 April 2024

Keywords:
Circulating tumor cells
Surface-enhanced Raman scattering
PD-L1
Iron oxide bioprobe
Dual-modal imaging
Tumor boundaries delineation

ABSTRACT

Early diagnosis and accurate boundary delineation are the key steps of tumor precision medicine. Circulating tumor cells (CTCs) detection of liquid biopsy can provide abundant information for early diagnosis of cancer. High detection specificity and good enrichment features are two key factors for CTCs accurate identification in peripheral blood sample. For this purpose, iron oxide (IO)-based surface-enhanced Raman scattering (SERS) bioprobes with good biocompatibility, high detection sensitivity, remarkable detection specificity, and good enrichment efficiency, were developed for detecting different types of CTCs. Magnetic SERS bioprobes combined with programmed death ligand-1 (PD-L1) antibody are regarded as an effective way to boost the targeting ability and detection specificity, benefiting for accurately capturing and identifying rare CTCs. Four types of CTCs with different PD-L1 expression were accurately distinguished among white blood cells *via* high-resolution SERS mapping images and stable Raman signals. Subsequently, CTCs blood samples obtained from the triple negative breast cancer patients were also successfully recognized compared to that of health people, indicating IO@AR@PDA-aPD-L1 SERS bioprobe possessed great potential for CTCs detection in liquid biopsy. Additionally, IO-based bioprobe exhibited excellent dual-modal imaging abilities of high-resolution SERS imaging mode and microimaging magnetic resonance imaging mode. These two highly complementary imaging modes endowed IO-based bioprobes unrivalled capacity in tumor boundary differentiation, supporting tumor accurate resection and precise surgery. To our best knowledge, this is the first time that biocompatible IO-based SERS bioprobes without noble metal element were reported not only for CTCs accurate detection, but also for precise tumor boundary delineation, showing great advantages in tumor diagnosis and treatment.

Patients with advanced malignant tumors have a short survival cycle and low quality of life [1]. Early diagnosis and treatment are effective ways to improve the life quality, reduce mortality, and improve prognosis of cancer patients [2]. Current areas of diagnostic imaging of tumors screening [3,4] combined with pathological biopsy are mainly by visualization methods [5–7]. However, the uncertainty of imaging diagnosis of tumor [8–10] and the invasive nature of pathological biopsy limit the early detection of tumor to some extent [11–13]. After the tumor is found, it needs to be treated, and there is no doubt that surgery is the most important cure for early tumor [14,15]. However, during the operation, the boundary between the tumor and the normal tissue is often difficult to distinguish, resulting in excessive excision of the normal tissue or incomplete excision of the tumor tissue, which leads to overtreatment or tumor recurrence [16]. Therefore, early diagnosis and accurate boundary differentiation of tumors is an immediate challenge, which plays a crucial role in tumor precision medicine [17]. Programmed death ligand-1 (PD-L1)-guided immunotherapy [18–20] is a major research hotspot [21], mainly because of the

* Corresponding authors.
E-mail addresses: xiaoxiawu@ucas.ac.cn (X. Wu), linjie@nimte.ac.cn (J. Lin), aiguo@nimte.ac.cn (A. Wu), shaogl@zjcc.org.cn (G. Shao).
[1] These authors contributed equally to this work.

https://doi.org/10.1016/j.cclet.2024.109857
1001-8417/

PD-L1-positive tumor patients will significantly benefit from immunotherapy [22–25]. Significantly, PD-L1 antibody (aPD-L1) utilized in bioprobe can largely boost tumor detection specificity and targeting ability, achieving accurate and reliable diagnostic results.

Circulating tumor cells (CTCs) existed in the peripheral blood, are cancer cells shed from the primary tumor [26]. CTCs enter the bloodstream and lymph and will metastasize to distant tissues through the bloodstream [27]. As a liquid biomarker for biopsy, CTCs have the advantages of good patient compliance, simple sampling operation, and high specificity [28,29]. For clinical diagnostic purposes, CTCs detection can acquire abundant information about tumorigenesis, metastasis, progression, and drug resistance, which is beneficial for monitoring tumor development and predicting tumor treatment efficacy [28–33]. Several efficient detection techniques with high sensitivity characteristics [29,34] are explored for CTCs detection due to extremely low concentration of CTCs in the blood with ~1–10 CTCs/mL [35]. Surface-enhanced Raman scattering (SERS) bioprobes have the unique advantages of fingerprint spectra, high sensitivity, good signal stability, and nondestructive testing mode [36–40], presenting great application potential in CTCs detection [41,42]. Recently, CTCs detection is important for guiding treatment protocols and assessing prognosis as a non-invasive strategy, it can be a guide to whether to administer immunotherapy to patients with advanced cancer [43–45]. Based on the above reported works, exploring novel SERS bioprobes with high detection specificity, and excellent targeting ability are the key premise for CTCs accurate detection. In addition, CTCs capture rate will be obviously promoted *via* magnetic SERS bioprobes under the magnetic field, resulting in high efficiency enrichment of CTCs.

Combining magnetic SERS bioprobes of iron oxide nanoparticles (IO NPs) with aPD-L1 is an effective way to improve the targeting ability and detection specificity [46,47], which is beneficial to improve the detection accuracy of different types of CTCs. SERS signal/mapping images can provide rich tumor diagnostic information obtained through CTCs detection *in vitro* [48]. Besides, magnetic SERS bioprobes not only have great advantages in the field of CTCs detection [29,43,49], but also can presents a good application prospect in the surgical treatment [38,50–52]. Importantly, aPD-L1 with high detection specificity will also make a great contribution in tumor boundary delineation [53]. As we all know, magnetic nanomaterials have the function of magnetic resonance imaging (MRI) enhancement due to the superparamagnetic effect of ferric tetroxide and small size of the diameter [54,55], by increasing the relaxation rate of hydrogen protons in the water molecules of the surrounding tissue. The contrast between the targeted region and the background tissue can be significantly enhanced by introducing iron tetroxide [54,56], thus improving the imaging sensitivity. Although MRI can well display the tumor lesion site [57] and play a crucial part in the microimaging of solid tumors [58,59], the limited imaging resolution cannot satisfy the requirement of the boundary distinction between tumor and normal tissue. Hence, developing high resolution imaging mode to delineating tumor boundary is an urgent task for supporting tumor accurate resection. Pure IO NPs as bioprobes have been reported with excellent SERS-MRI dual-modal imaging abilities [60], IO NPs modified with PD-L1 antibody will endow bioprobes excellent detection specificity, which maybe a viable approach to achieve precise tumor boundary delineation *in vitro*.

Herein, we utilized aPD-L1 to develop IO@AR@PDA-aPD-L1 SERS bioprobes with unique detection sensitivity, good biocompatibility, and remarkable magnetic enrichment. In this study, ultrasmall sized IO NPs were prepared by solvothermal method, and then linked with Raman reporter of alizarin red (AR) to synthesize IO@AR nanoparticles shown in Scheme 1. Next, polydopamine (PDA) was modified on IO@AR to improve its stability, and offered sufficient reaction sites to conjugate targeting molecule. Finally, PDA modified IO@AR nanoparticles (IO@AR@PDA NPs) was further conjugated with aPD-L1 to create IO@AR@PDA-aPD-L1 SERS bioprobe. The high detection specificity and excellent targeting ability of this SERS bioprobe were endowed by aPD-L1, largely boosting the CTCs detection accuracy. Four different types of CTCs were accurately distinguished from white blood cells (WBCs) in peripheral blood sample *via* IO-based SERS imaging/signals, and SERS mapping imaging and Raman signals for CTCs were intense and stable. Besides, CTCs with high PD-L1 expression from triple negative breast cancer (TNBC) patients were successfully identified by IO-based SERS bioprobe compared to that of health people. TNBC blood exhibited distinct SERS signals, and no obvious signals was observed in healthy human blood. Importantly, high-resolution SERS imaging mode and micro-MRI mode were developed in IO-based bioprobes and tumor boundary delineation was successfully achieved by the SERS-MRI dual-modal imaging modes. High-resolution and highly specific SERS imaging technique combined with MR imaging displayed huge potential in tumor diagnosis and operative treatment. To our best knowledge, this is the first report that IO-based SERS bioprobes without noble metal element simultaneously utilized in CTCs detection and tumor boundary delineation. This IO-based SERS biopobe can not only achieve accurate CTCs detection but also guide tumor accurate resection, improving tumor diagnostic and therapeutic effects.

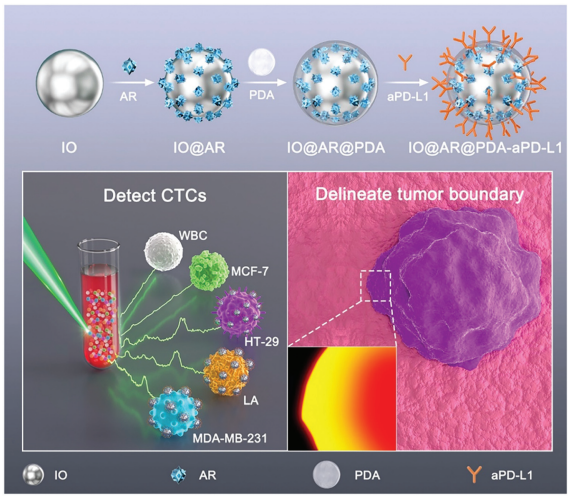

Scheme 1. Illustration of PD-L1 targeted SERS bioprobes to detect CTCs in peripheral blood and delineate the tumor boundary in tumor tissues.

The synthesis of SERS bioprobe (IO@AR@PDA-aPD-L1) was shown in Scheme 1. Upon IO NPs synthesis, water-soluble IO NPs were obtained by oil-to-water conversion of citric acid. As shown in Fig. 1a and Figs. S1a–c (Supporting information), ultra-small IO NPs with a uniform size of 7–9 nm had a clear lattice plane. The interplanar distance of IO NPs was 0.252 nm matched to crystal face of (3 1 1) [60]. Then AR Raman reporter molecules were modified on IO NPs to obtain stable Raman signal shown in transmission electron microscopy (TEM) image (Fig. 1b). According to SERS signals and stabilities of as-prepared IO-based substrates, the concentration of AR was optimized using confocal Raman spectroscopy under excitation of 532 nm laser shown in Fig. S2 (Supporting information). Subsequently, 5×10^{-4} mol/L was determined to be the final AR concentration for SERS bioprobe synthesis. In Fig. 1c, IO@AR NPs were coated with PDA to improve biocompatibility and stability of nanoparticles, which also provided sufficient binding sites for aPD-L1 conjugation [61,62]. From TEM images, we could find the presence of PDA layer on the IO NPs surface, indicating the successful modification of PDA using Schiff Base reac-

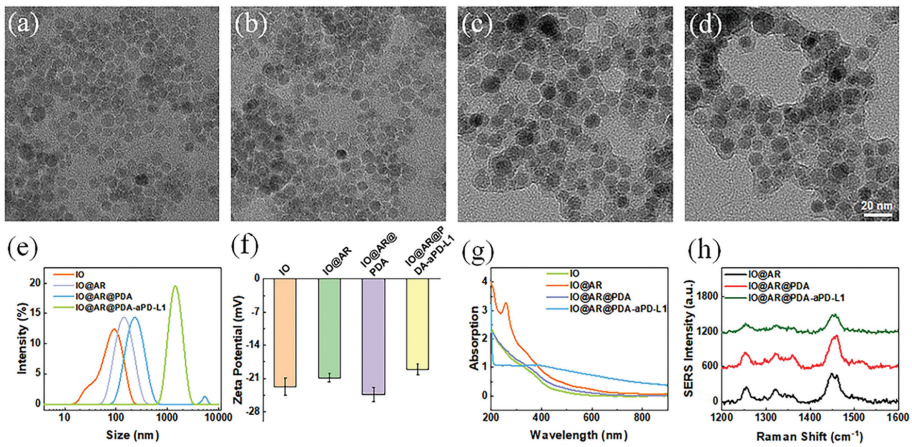

Fig. 1. (a–d) TEM images of IO, IO@AR, IO@AR@PDA and IO@AR@PDA-aPD-L1 NPs. (e, f) The size distributions and zeta potentials of IO, IO@AR, IO@AR@PDA, IO@AR@PDA-aPD-L1 NPs tested by DLS at room temperature. Data are presented as mean ± standard deviation (SD) ($n = 3$). (g) UV–vis spectra of IO, IO@AR, IO@AR@PDA and IO@AR@PDA-aPD-L1 NPs. (h) SERS spectra of IO@AR, IO@AR@PDA and IO@AR@PDA-aPD-L1 bioprobes. Laser wavelength: 532 nm; laser power: 2.68 mW; lens: 50× objective.

tion. Next, aPD-L1 molecules were linked to IO@AR@PDA NPs to prepare IO@AR@PDA-aPD-L1 SERS bioprobe (Fig. 1d). Similarly, the IO-based SERS bioprobe was equipped to efficiently target PD-L1-overexpressing cells and tumor tissues. From high-angle annular dark-field STEM (HAADF-STEM) and elemental mapping (N/O/S/Fe) images in Fig. S3 (Supporting information), it could be found that the as-prepared SERS bioprobe consisted of S of AR, N of PDA, and Fe of IO NPs, further confirming that AR was linked to IO NPs, and IO@AR NPs was coated with PDA layer. Meanwhile, the size distributions and zeta potentials of different nanoparticles during synthesis were shown in Figs. 1e and f and Fig. S4 (Supporting information). The IO nanoparticles have good dispersibility and size distribution of 11.13 ± 1.63 nm in cyclohexane shown in Fig. S4 of dynamic light scattering (DLS) test. But IO nanoparticles are-prone to agglomeration during the conversion from oil phase to the aqueous phase, which leading to a larger size in DLS result. Owing to modifications with AR, PDA, and aPD-L1, the hydrodynamic sizes of nanoparticles were increased, and the surface potentials of nanoparticles were also changed accordingly. Nevertheless, all nanoparticles were negatively charged, attributed to modification with sodium citrate in the oil-to-water conversion of IO NPs and free hydroxyl groups in PDA molecules [63]. Additionally, the Schiff base reaction, which is responsible for cross-linking of aPD-L1, led to increased potential of nanoparticles because of huge consumption of hydroxyl groups [64].

Fig. 1g showed the ultraviolet–visible spectroscopy (UV–vis) spectra of different nanoparticles during synthesis. The absorption peaks changed after modifications of AR, PDA, and aPD-L1. It could be observed that absorption peak at 260 nm was the characteristic peak of AR, indicating successful modification of AR molecules. Specifically, this characteristic peak was drastically reduced after PDA coating and antibody linking, the Raman signals spectra in Fig. 1h also gradually weakened, suggesting that the PDA coating layer weakened AR molecules' Raman signals. As above results shown, the Raman signals of IO NPs-based SERS nanoparticles were reduced with each subsequent step of modification. Nevertheless, the final signal intensity was enough for Raman detection/imaging. Moreover, confocal laser scanning microscopy (CLSM) was also utilized to verify whether aPD-L1 was successfully linked to bioprobe in Fig. S5 (Supporting information). We used Alexa Fluor 488-labeled aPD-L1 to prepare SERS bioprobe of IO@AR@PDA-aPD-L1–488 NPs by the same method. It was found that the brightfield and fluorescence image of the IO@AR@PDA-aPD-L1–488 bioprobe superimposed and matched perfectly. This result indicated the successful conjugation of aPD-L1 with the IO-based SERS bioprobe using Schiff Base reaction, suggesting that it exhibited huge potential to perform CTCs detection using this SERS bioprobe.

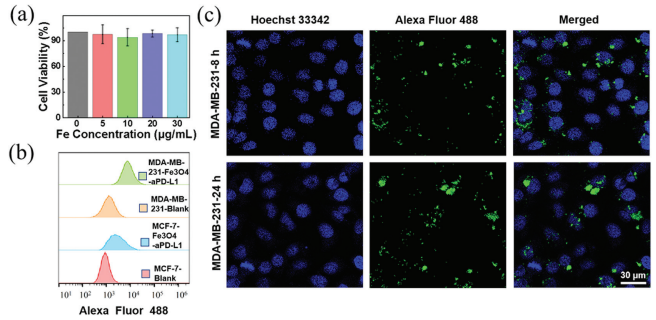

Fig. 2. (a) Biocompatibility of IO@AR@PDA-aPD-L1 bioprobes incubated with MDA-MB-231 cells. Data are presented as mean ± SD ($n = 3$). (b) Flow cytometry analysis of MDA-MB-231 cells incubated with Alexa Fluor 488-labeled SERS bioprobes. (c) CLSM images of MDA-MB-231 cells incubated with IO@AR@PDA-aPD-L1–488 for 8 and 24 h, respectively. The cells were treated with Hoechst 33342 (Em: 430–490 nm; Ex: 405 nm), and IO@AR@PDA-aPD-L1–488 were excited at the wavelength of 488 nm, and the fluorescence images at emission wavelengths were at 500–550 nm.

The biocompatibility of the SERS bioprobe was first investigated *in vitro* using the triple-negative breast cancer cell lines (MDA-MB-231 cells) after the synthesis of the bioprobe. As shown in Fig. 2a, there was no significant decrease in cell viabilities incubated with different concentrations of SERS bioprobe for 24 h, indicating that the SERS bioprobe was biosafety. Meanwhile, the cellular uptake of SERS bioprobes were also investigated using CLSM and flow cytometry. As shown in Figs. 2b and c and Fig. S6 (Supporting information), flow cytometry and CLSM results showed that the cellular uptake of SERS bioprobe in MDA-MB-231 cells increased with time going, and was significantly higher than that in MCF-7 cells due to the higher PD-L1 expression in MDA-MB-231 cells [65]. These results verified that our SERS bioprobe had great biocompatibility and specific targeting ability to cancer cells with high PD-L1 expression, which could be used in CTCs accurate detection.

Additionally, high-resolution SERS mapping image was further observed to evaluate targeting ability and cellular uptake of SERS bioprobe. After incubation with the IO@AR@PDA-aPD-L1 bioprobe, SERS mapping results showed that MDA-MB-231 cells possessed prominent SERS signals with increased incubation time (Figs. 3a and b). In Figs. 3c and d, the SERS signals at 24 h were significantly higher than those at 8 h in four randomly selected points

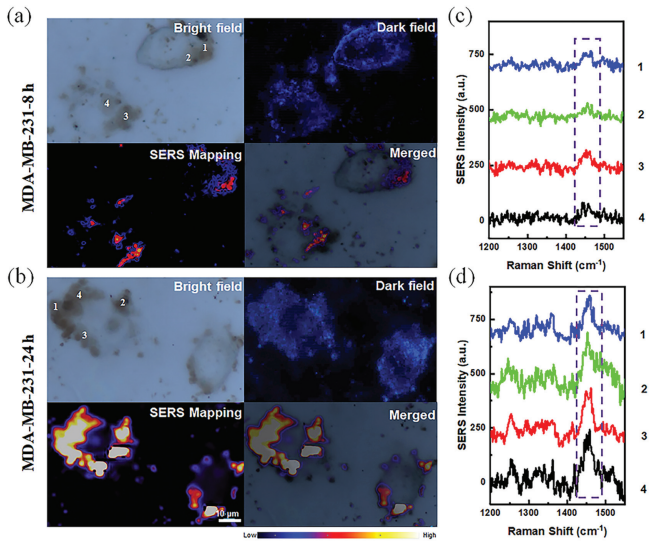

Fig. 3. (a, b) Bright filed, dark field and SERS mapping images of MDA-MB-231 cells incubated with IO@AR@PDA-aPD-L1 bioprobes for 8 and 24 h, respectively. (c, d) SERS spectra of random 4 points collected from left MDA-MB-231 cells. Laser wavelength: 532 nm; laser power: 2.68 mW; lens: 50× objective.

from SERS mapping images. In contrast to MCF-7 cells with low PD-L1 expression (Figs. S7a and b in Supporting information) [65], MCF-7 cells showed almost no SERS signals and bioprobe uptake, but a small amount of adsorption over time, up to 24 h. It has been demonstrated that SERS mapping results were consistent with the CLSM and flow cytometry results, further confirming specific targeting ability and high sensitivity of this SERS bioprobe.

All animal procedures were performed in accordance with the Guidelines for the Care and Use of Laboratory Animals of Chinese Experimental Animals Administration Legislation and approved by the Animal Ethics Committee of Medical College of Ningbo University (SYXK (Zhe) 2019–0005). Given the excellent PD-L1 targeting and cellular uptake ability of the SERS bioprobe, it was used to detect CTCs subsequently. We used the SERS bioprobe to detect cancer cells of HT-29, lung adenocarcinoma (LA), MDA-MB-231, and MCF-7 cells in rabbit blood to investigate the SERS bioprobe's detection specificity. As shown in Figs. 4a–d of bright fields and SERS mapping images, the results showed that the SERS signals of the three cells (HT-29, LA and MDA-MB-231 cells) with high PD-L1 expression [65–67] were more obvious in the SERS mapping images, and consistent with the SERS spectra obtained by randomly selecting six points on the cells. In contrast, there was no obvious signal in the SERS mapping images and corresponding spectra for MCF-7 cells and WBCs in the blood due to their low PD-L1 expression. Therefore, this SERS bioprobe exhibited good specificity for detecting tumor cells with high PD-L1 expression in peripheral blood. Moreover, the detection sensitivity of SERS bioprobe was also investigated in the rabbit blood model. Figs. 4e–g and Figs. S8 and S9 (Supporting information) showed the CTCs detection of rabbit blood samples with different numbers of cancer cells (2–500 cells/mL). There were still quite obvious SERS signals in 2 cells/mL blood samples for cells (HT-29, LA and MDA-MB-231 cells) with high PD-L1 expression level, indicating that the limit of detection could be as low as 2 cells/mL. Thus, it could be concluded that the designed SERS bioprobe had high specificity and sensitivity in CTCs detection.

We have also utilized the SERS bioprobe to further test clinical blood samples after achieving the high specificity and sensitivity of CTCs detection in rabbit blood. Human blood experiments were supported by the Zhejiang Cancer Hospital, and the treatment

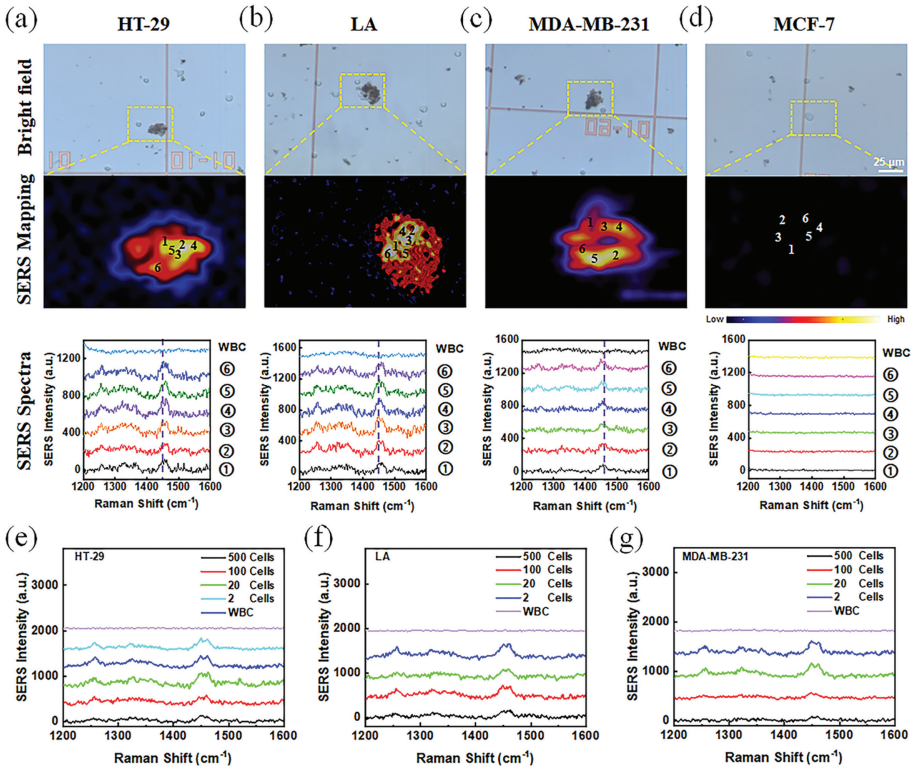

Fig. 4. (a–d) Bright filed, SERS mapping, and the related SERS spectra of above captured cancer cells of HT-29 (a), LA (b), MDA-MB-231 (c) and MCF-7 (d) cells from rabbit peripheral blood using IO@AR@PDA-aPD-L1 bioprobes. (e–g) The detection sensitivities of IO@AR@PDA-aPD-L1 bioprobes for HT-29, LA and MDA-MB-231 cells in blood. Laser wavelength: 532 nm; laser power: 11.625 mW; lens: 10× objective.

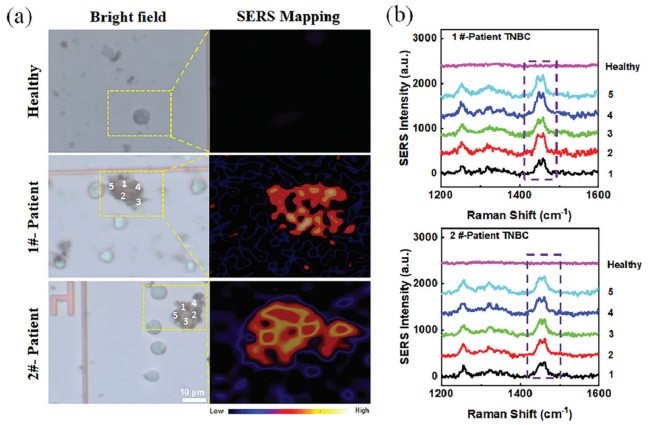

Fig. 5. CTCs detection of blood samples from healthy person and TNBC patients. (a) The bright field and SERS mapping images of captured cells from blood of healthy person and TNBC patients. (b) The corresponding SERS spectra of left captured cells. Laser wavelength: 532 nm; laser power: 11.625 mW; lens: 10× objective.

process of blood samples was implemented according to the quality management standards of the Blood Station Laboratory. Human blood samples were drawn from the cubital veins of breast cancer patients, and then injected into disposable vacuum blood collection vessels containing heparin sodium. As a control group, the blood samples of healthy people were obtained in the same way and the treatment process was as follows: 2 mL blood sample was diluted with 2 mL PBS, then slowly added to 2 mL of the human blood lymphocyte isolation medium and centrifuged immediately for 25 min at 1500 rpm. As shown in Fig. 5, blood samples from healthy individuals and two TNBC patients were measured using SERS bioprobes. It seemed that there were no obvious SERS mapping images/Raman signals in healthy human blood in Figs. 5a and b. On the contrary, the cells with obvious SERS mapping images were captured and detected in the blood samples from TNBC patients (Fig. 5a), and the results were further verified by their corresponding SERS spectral signals (Fig. 5b). Therefore, this SERS bioprobe possessed very high specificity and sensitivity for CTCs detection, and displayed great potential to detect CTCs with high PD-L1 expression in liquid biopsy.

The biosafety of SERS bioprobe was further investigated in mouse model. SERS bioprobe was injected *via* the tail vein, and 14 days later, tissue slices of major organs (heart, liver, spleen, lungs, kidneys) were collected and analyzed by hematoxylin-eosin (H&E) staining. Fig. S10 (Supporting information) showed the SERS bioprobe did not cause significant damage to the mice's organs. Meanwhile, blood markers were also analyzed on day 14 (Fig. S11 in Supporting information). It could be found that there was no discernible difference between the bioprobe and control groups, indicating that the SERS bioprobe did not cause significant toxicity. Overall, the SERS bioprobe exhibited good biocompatibility and could be used for *in vivo* tumor MRI imaging and boundary delineation.

Firstly, *in vitro* and *in vivo* enhanced MR imaging capabilities of our bioprobe based on superparamagnetic IO substrates were evaluated. In Fig. S12 (Supporting information), T_1 and T_2 MR imaging results suggested that the SERS bioprobe had good bimodal MR imaging capability. After injecting the bioprobe *via* the tail vein in tumor-bearing mice, subcutaneous tumor (MDA-MB-231 and MCF-7 cells) were recorded at different time points using MR imaging equipment under the magnetic field of 3.0 T. Fig. 6a and Figs. S13 and S14 (Supporting information) showed enhanced darker signals of MDA-MB-231 tumor than that in MCF-7 tumor, it could be found clearly distinguishes of tumor from normal tissues after 2 h tail vein injection. Eventually, the tumor was gradually brightened up due to the gradual metabolism of the bioprobe. Therefore, MR imaging of PD-L1-overexpressing tumors could be achieved using the MRI-SERS bioprobe, which effectively decreased the pain and risk of biopsy sampling in tumor diagnosis.

To further delineate the tumor boundary with higher resolution and accuracy, IO@AR@PDA-aPD-L1 bioprobe was injected into the subcutaneous tumors with high PD-L1 expression of MDA-MB-231 and HT-29 cells [65,66]. Two hours later, tumor tissues were removed and sliced, and finally examined using a confocal Raman microscopy. As shown in Figs. 6b and c, high-resolution SERS mapping scanning was performed by selecting a region (shown by the red dashed box in the SERS bright field image). The boundary be-

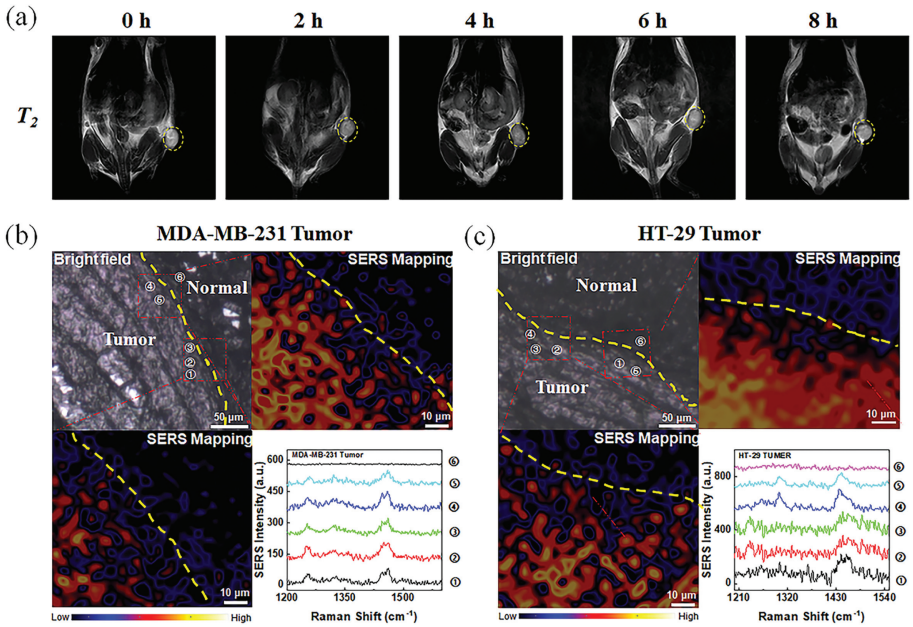

Fig. 6. (a) T_2-weighted images of MDA-MB-231 cells tumor bearing mice at different time points under the 3.0 T magnetic field. (b, c) Bright field, SERS mapping, and corresponding SERS spectra of tissues from MDA-MB-231 and HT-29 tumors of tumor bearing mice with IO@AR@PDA-aPD-L1 bioprebes treatment, respectively. Laser wavelength: 532 nm; laser power: 12.05 mW; lens: 5× objective.

tween tumor tissues and normal tissues was shown clearly, with strong signals on SERS mapping images and the corresponding SERS spectra in the tumor tissues region. In sharp contrast, there were no obvious signals on SERS mapping images and spectra signals in normal tissues. Therefore, the accuracy of tumor boundary delineation could be improved by using SERS technology, and the SERS bioprobes possessed high specificity and sensitivity in delineating PD-L1-positive tumor boundary [68]. Overall, the developed IO@AR@PDA-aPD-L1 bioprobe has the bifunctional detection capabilities of SERS-MRI in high-expression PD-L1 tumors. This IO-based SERS bioprobe is expected to be applied to non-invasive liquid biopsy in diagnosis of PD-L1 expression tumors, and visualization of tumor boundary delineation with high resolution, leading to improved precise medicine and better patient treatment [69–71].

In conclusion, IO@AR@PDA-aPD-L1 SERS bioprobe were successfully developed for accurate detection of CTCs and precise delineation of tumor boundary. IO-based SERS bioprobe exhibited high detection sensitivity, good biocompatibility, and magnetic enrichment characteristics. The detection specificity and tumor targeting ability were largely improved by modifying aPD-L1 on the surface of SERS bioprobe. Thus, four different types CTCs were accurately distinguished with the remaining WBCs by the obvious SERS images and intense Raman signals by the designed SERS bioprobes. The peripheral blood samples from two TNBC patients were accurately recognized by the distinct SERS signals compared to that of health people. Besides, IO-based SERS bioprobe exhibited SERS-MRI dual-modal imaging capabilities, these two highly complementary imaging modes displayed tremendous advantages in tumor diagnosis and treatment. Moreover, high-resolution and good specificity SERS image technology was utilized for tumor boundary precise delineation, which supporting tumor accurate resection and precision surgery. In short, the IO-based SERS bioprobe proposed in this work is of great potential for the clinical CTCs detection of PD-L1-overexpressing tumor, and it is expected to be employed as a molecular image bioprobe with SERS-MRI dual-modal image ability, guiding tumor surgical resection and immunotherapy.

Ethical statement

All experiments were performed in accordance with the Guidelines of the Ministry of Health of the People's Republic of China (Document No. 55, 2001), and the human subject experiments were approved by the Ethics Committee at Zhejiang Cancer Hospital (XF20170545) and conducted according to the principles of the Declaration of Helsinki. Informed consent was obtained from human participants of this study.

Declaration of competing interest

The authors declare that they have no known competing financial interests or personal relationships that could have appeared to influence the work reported in this paper.

CRediT authorship contribution statement

Ting Pan: Writing – review & editing, Writing – original draft, Investigation. **Dinghu Zhang:** Formal analysis, Investigation, Methodology, Project administration, Writing – original draft, Writing – review & editing. **Guomei You:** Formal analysis, Software, Validation, Writing – original draft, Writing – review & editing. **Xiaoxia Wu:** Writing – review & editing, Writing – original draft, Investigation, Methodology, Project administration, Supervision. **Chenguang Zhang:** Validation, Methodology, Investigation, Formal analysis, Data curation. **Xinyu Miao:** Visualization, Validation, Methodology, Formal analysis. **Wenzhi Ren:** Writing – review & editing, Validation, Project administration. **Yiwei He:** Writing – review & editing, Visualization, Methodology, Investigation. **Lulu He:** Validation, Resources, Investigation. **Yuanchuan Gong:** Visualization, Methodology, Data curation, Writing – review & editing. **Jie Lin:** Supervision, Writing – original draft, Writing – review & editing, Conceptualization, Methodology, Project administration. **Aiguo Wu:** Writing – review & editing, Writing – original draft, Project administration, Funding acquisition, Conceptualization. **Guoliang Shao:** Conceptualization, Funding acquisition, Investigation, Project administration, Supervision, Writing – original draft, Writing – review & editing.

Acknowledgments

This work was supported by the funding from National Natural Science Foundation of China (Nos. 32025021, 12374390, 31971292, 82072032, 82202274), Ningbo 3315 Innovative Teams Program (No. 2019A-14-C), The member of Youth Innovation Promotion Association Foundation of CAS (No. 2023310), Key Scientific and Technological Special Project of Ningbo City (Nos. 2023Z209, 2020Z189), National Key R&D Program of China (No. 2019YFA0405603), Provincial Natural Science Foundation of Zhejiang (Nos. LQ23H180007, LQ23H180003), Zhejiang Province Science and Technology Plan of Traditional Chinese Medicine (No. 2021KY085), Zhejiang Provincial Traditional Chinese Medicine Foundation (No. 2021ZB04), and the Major Medical and Health Science and Technology Project of Zhejiang Province (No. WKJ-ZJ-2002).

Supplementary materials

Supplementary material associated with this article can be found, in the online version, at doi:10.1016/j.cclet.2024.109857.

References

[1] K. Wang, L. Xiong, Z. Zhang, et al., J. Cent. South Univ. 44 (2019) 1275–1280.
[2] A. Llombart-Cussac, Breast Cancer Res. Treat. 112 (2008) 15–24.
[3] C.L. Shen, T.C. Jiang, Q. Lou, et al., SmartMat 3 (2022) 269–285.
[4] H. Jiang, Q. Chen, H. Wang, et al., Chin. Chem. Lett. 35 (2024) 108899.
[5] D.P. Winchester, J.M. Jeske, R.A. Goldschmidt, CA. Cancer J. Clin. 50 (2000) 184–200.
[6] R. Alcantara, M. Posso, M. Pitarch, et al., Eur. Radiol. 33 (2023) 417–428.
[7] P. Puech, O. Rouvière, R. Renard-Penna, et al., Radiology 268 (2013) 461–469.
[8] X. Fave, M. Cook, A. Frederick, et al., Comput. Med. Imaging Graph. 44 (2015) 54–61.
[9] P.A. Carney, J.P. Yi, L.A. Abraham, et al., J. Gen. Intern. Med. 22 (2007) 234–241.
[10] D.L. Daniels, S.J. Millen, G.A. Meyer, et al., AJR. Am. J. Roentgenol. 148 (1987) 1219–1222.
[11] E.D. Poggio, R.L. McClelland, K.N. Blank, et al., Clin. J. Am. Soc. Nephrol. 15 (2020) 1595–1602.
[12] D.B. Asante, L. Calapre, M. Ziman, et al., Cancer Lett. 468 (2020) 59–71.
[13] B.M. Blokker, I.M. Wagensveld, A.C. Weustink, et al., Eur. Radiol. 26 (2016) 1159–1179.
[14] F. MacNeill, A. Karakatsanis, Breast 31 (2017) 284–289.
[15] W. Hartwig, J. Werner, D. Jäger, et al., Lancet Oncol. 14 (2013) e476–e485.
[16] N. Harbeck, M. Gnant, Lancet 389 (2017) 1134–1150.
[17] P. Janiaud, S. Serghiou, J.P.A. Ioannidis, Cancer Treat. Rev. 73 (2019) 20–30.
[18] D. Jin, X.X. Peng, Y. Qin, et al., Anal. Chem. 92 (2020) 9877–9886.
[19] Q. Gou, C. Dong, H. Xu, et al., Cell Death Discov. 11 (2020) 955.
[20] T.A. Chan, M. Yarchoan, E. Jaffee, et al., Ann. Oncol. 30 (2019) 44–56.
[21] X. Zhou, T. Ren, H. Zan, et al., Front. Immunol. 13 (2022) 864202.
[22] Y. Wang, K.C.C. Johnson, M.E. Gatti-Mays, J. Hematol. Oncol. 15 (2022) 118.
[23] J. Huynh, K. Patel, J. Gong, et al., Curr. Treat. Options Oncol. 22 (2021) 100.
[24] X. Dai, Y. Gao, W. Wei, Semin. Cancer Biol. 85 (2022) 246–252.
[25] D. Atanackovic, T. Luetkens, Semin. Cancer Biol. 52 (2018) 198–206.
[26] D. Lin, L. Shen, M. Luo, et al., Signal Transduct. Target. Ther. 6 (2021) 404.
[27] Z. Shen, A. Wu, X. Chen, Chem. Soc. Rev. 46 (2017) 2038–2056.
[28] H. Ruan, X. Wu, C. Yang, et al., ACS Biomater. Sci. Eng. 4 (2018) 1073–1082.
[29] Y. Xu, J. Lin, X. Wu, et al., J. Mater. Chem. B 10 (2022) 3808–3816.
[30] X. Wu, Y. Xia, Y. Huang, et al., ACS Appl. Mater. Interfaces 8 (2016) 19928–19938.
[31] Y. Xu, D. Zhang, J. Lin, et al., Biomater. Sci. 10 (2022) 1812–1820.
[32] Z.W. Sun, Y.Y. Jiang, M. Stenzel, SmartMat 2 (2021) 127–130.
[33] H. Hu, W. Zhang, L. Lei, et al., Chin. Chem. Lett. 35 (2024) 108765.
[34] X. Wu, L. Luo, S. Yang, et al., ACS Appl. Mater. Interfaces 7 (2015) 9965–9971.
[35] M.Nora Dickson, P. Tsinberg, Z. Tang, et al., Biomicrofluidics 5 (2011) 034119.

[36] H. Liu, X. Gao, C. Xu, et al., Theranostics 12 (2022) 1870–1903.
[37] X.Y. Meng, L. Qiu, G.C. Xi, et al., SmartMat 2 (2021) 466–487.
[38] Z.Y. Wang, J. Mei, D.Q. Ni, et al., Rare Met. 42 (2023) 1483–1493.
[39] G.C. Zheng, I. Pastoriza-Santos, J. Perez-Juste, et al., SmartMat 2 (2021) 446–465.
[40] Q. Yang, Y.Y. Mao, Q. Liu, et al., Rare Met. 42 (2023) 2928–2948.
[41] L.E. Jamieson, S.M. Asiala, K. Gracie, et al., Annu. Rev. Anal. Chem. 10 (2017) 415–437.
[42] S. Zhu, B. Deng, F. Liu, et al., ACS Appl. Mater. Interfaces 14 (2022) 8876–8887.
[43] X. Xu, J. Lin, Y. Guo, et al., Biosens. Bioelectron. 210 (2022) 114305.
[44] R.E. Wilson Jr., R. O'Connor, C.E. Gallops, et al., ACS Appl. Mater. Interfaces 12 (2020) 47220–47232.
[45] M. He, J. Lin, O.U. Akakuru, et al., Sci. China Life Sci. 65 (2022) 561–571.
[46] Y. Zhou, Q. Chen, S. Zhong, et al., Biosens. Bioelectron. 237 (2023) 115493.
[47] E. Feng, T. Zheng, X. He, et al., Sci. Adv. 4 (2018) eaau3494.
[48] J. Li, Y. Li, P. Li, et al., Acta Biomater. 144 (2022) 1–14.
[49] J. Lin, J. Zheng, A. Wu, J. Mater. Chem. B 8 (2020) 3316–3326.
[50] E. Lenzi, D. Jimenez de Aberasturi, L.M. Liz-Marzán, ACS Sens. 4 (2019) 1126–1137.
[51] Y. Li, Z. Wang, X. Mu, et al., Biotechnol. Adv. 35 (2017) 168–177.
[52] W. Duan, Q. Yue, Y. Liu, et al., Chem. Sci. 11 (2020) 4397–4402.
[53] A. Samanta, S. Jana, R.K. Das, et al., Nanomedicine 9 (2014) 523–535.
[54] P.J. Mergo, J.D. Engelken, T. Helmberger, et al., Imaging 8 (1998) 1073–1078.
[55] J.W. Bulte, T. Douglas, S. Mann, et al., J. Magn. Reson. Imaging 4 (1994) 497–505.
[56] P. Reimer, B. Tombach, Eur. Radiol. 8 (1998) 1198–1204.
[57] F.E. Azami Hassani, F. Slimani, Ann. Med. Surg. 63 (2021) 102187.
[58] M. Sumi, M. Van Cauteren, T. Nakamura, AJR. Am. J. Roentgenol. 186 (2006) 749–757.
[59] D. Artemov, G. Revelon, E. Atalar, et al., Magn. Reson. Med. 41 (1999) 569–574.
[60] J. Lin, X. Ma, A. Li, et al., Fund. Res. 4 (2024) 858–867.
[61] G.C. Wang, P. Huang, L. Wang, et al., SmartMat 3 (2022) 522–531.
[62] J. An, C.Y. Zhao, Z.J. He, et al., Rare Met. 41 (2022) 3351–3359.
[63] T.T. Zhu, H. Wang, H.W. Gu, et al., J. Nanobiotechnol. 21 (2023) 52.
[64] H.J. Cho, S.K. Perikamana, J.H. Lee, et al., ACS Appl. Mater. Interfaces 6 (2014) 11225–11235.
[65] S. Heskamp, W. Hobo, J.D. Molkenboer-Kuenen, et al., Cancer Res. 75 (2015) 2928–2936.
[66] C. Liu, Z. Yao, J. Wang, et al., Cell Death Differ. 27 (2020) 1765–1781.
[67] H. Yu, T.A. Boyle, C. Zhou, et al., J. Thorac. Oncol. 11 (2016) 964–975.
[68] J. Lin, D. Zhang, J. Yu, et al., Anal. Chem. 95 (2023) 4671–4681.
[69] L.L. Wu, X. Meng, Q. Zhang, et al., Chin. Chem. Lett. 35 (2024) 108663.
[70] Y. Cao, X. Ge, Y. Wei, et al., Chin. Chem. Lett. 35 (2024) 108672.
[71] Y. Chen, J. Zhu, J. Ding, et al., Chin. Chem. Lett. 35 (2024) 108706.